JOURNAL OF GEOPHYSICAL RESEARCH, VOL. 86, NO. B6, PAGES 4913–4928, JUNE 10, 1981

Seismic and Aseismic Deformation Associated With the 1952 Kern County, California, Earthquake and Relationship to the Quaternary History of the White Wolf Fault

ROSS S. STEIN[1]

Department of Geology, Stanford University, Stanford, California 94305
U.S. Geological Survey, Menlo Park, California 94305

WAYNE THATCHER

U.S. Geological Survey, Menlo Park, California 94305

Synthesis of geodetic, geologic, and seismic data from the White Wolf fault, California, indicates that the fault separates an area of late Quaternary and continuing rapid uplift in the Tehachapi Mountains and Transverse Ranges from even more rapid subsidence in the southern San Joaquin Valley. On July 21, 1952, rupture of the White Wolf fault produced the $M_L = 7.2$ Kern County earthquake. We used the aftershock zone to delimit the size of the faulted slip surface and applied constraints imposed by the known 1952–1953 horizontal shear strains to model the measured coseismic vertical displacements, with an elastic dislocation model. A curved fault trace with decreasing fault depth (27 to 10 km from the surface vertically to the base), slip (3 to 1 m), and dip (75° to 20°) from the 1952 epicenter at the southwest end of the fault toward the northeast provides the fit most consistent with the geodetic record, the measured seismic moment, the fault-plane solution, and the pattern of surface rupture. Two short releveled lines near the 1952 epicenter tilted 4 and 17 μrad down to the north from 5–10 years before the earthquake; the preseismic tilts differ significantly from ten other surveys of these lines. Left-lateral fault-crossing shear strain from 0.2–20 years before the quake was two times greater than both preseismic off-fault strains and the post-seismic fault-crossing strains. During the first seven years after the earthquake, aseismic deformation was negligible. From 1959 to 1972 uplift reached 160 mm over an area larger than the aftershock zone, rising first in the epicentral region and then at the northeast end of the fault. This was unaccompanied by any surface fault slip. Reconstruction of the vertical separation on the White Wolf fault from late Quaternary and late Miocene stratigraphic marker beds shows that the rate of reverse fault slip increased forty-fold, from 0.1–0.2 mm/yr to 3–9 mm/yr, between the past 10–15 m.y. and the most recent 0.6–1.2 m.y. We estimate a 170- to 450-yr average recurrence interval for earthquakes on the White Wolf fault with slip equivalent to that in 1952. The 1952 earthquake appears to be characteristic of the Quaternary record of fault displacement in the increase in White Wolf slip toward the San Andreas fault, the ratio of reverse to lateral slip (1.3:1), and the ratio of vertical fault slip to emergence of the hanging wall block (3:1). The >8500-m-deep sedimentary basin on the down-thrown block cannot be explained by repeated slip of the White Wolf fault in an elastic medium.

INTRODUCTION

About 5 to 10 years after the White Wolf fault ruptured during the $M_L = 7.2$ Kern County earthquake, a region of the southern California Transverse Ranges lying athwart the San Andreas fault's 'big bend' uplifted aseismically [*Castle et al.*, 1976; *Castle*, 1978]. Although the areal extent and precise timing of uplift is disputed by *Strange* [1981] and *Mark et al.* [1981], both authors concur that some uplift took place between 1959 and 1970, rising between 130 and 300 mm athwart the San Andreas fault's 'big bend' (Figure 1). The northwest bounding flexure of the southern California uplift of *Castle* [1978] approximately coincides with the White Wolf fault (Figure 1). These observations, together with the striking similarity between seismic and aseismic displacements along the fault to be presented in this paper, encourage the hypothesis that earthquakes on the White Wolf fault may be mechanically related to the uplift. If this hypothesis is valid, knowledge of the subsurface geometry and slip distribution of the 1952 Kern County earthquake provides an opportunity to investigate the process of rapid aseismic uplift and collapse, and to observe the relation between seismic and aseismic events. If the earthquake is related to the episode of aseismic uplift, then the depth of seismic displacements may provide a clue to the process of deformation.

The rate of uplift along the north and south margins of the western Transverse Ranges over time scales ranging from 48 to 600,00 years appears similar. The average historic rate of uplift near the White Wolf fault has been about 5–10 mm/yr since 1926. The sequence of uplifted marine terraces at the Ventura coastline along the southwest margin of the uplifted region allows assessment of older uplift. *Wehmiller et al.* [1977] found that both 2100- and 40,000-year-old terraces have risen at an average rate of 8–10 mm/yr (Figure 1, labeled MT). From age determinations of marine sedimentary rocks of the coastal Ventura Basin, whose location is shown in Figure 1 (labeled VB), *Yeats* [1977] estimated that the basin's north margin has risen at an average rate of 10 ± 2 mm/yr during the past 0.6 m.y. Between 1.2 and 0.6 m.y. B.P., the basin was subsiding. In contrast to the rapid uplift rate common to the western Transverse Ranges, the rate of coastal emergence north or south of the southern California uplift, measured both from tide gauges and marine terrace emergence, is at least an order of magnitude less than within the uplifted region [*Lajoie et al.*, 1979]. An important question then becomes

[1] Now at Lamont-Doherty Geological Observatory of Columbia University, Palisades, New York 10964.

Paper number 80B1831.

over what time interval has the White Wolf fault behaved as an active margin of uplift in the Tehachapi Ranges, and how has the rate of uplift along this margin varied in the past several million years?

Fortunately, a wealth of geodetic, geophysical, and geologic data is available for the 1952 earthquake and the region adjoining the White Wolf fault. We present results from an extensive precise (first order) leveling net that traverses the White Wolf fault at four points and spans the period 1926 to 1972, and a fault-crossing triangulation net from which horizontal strains can be deduced for periods before, during, and after the earthquake. Fault depth, dip, and slip associated with the 1952 earthquake are constrained by modeling the surface strains with a multiple fault three-dimensional elastic dislocation model, supported by comparison of the predicted and measured seismic moment, fault plane solution, pattern of ground rupture, and depth to granitic basement. Oil well logs and stratigraphic relationships are used to obtain Miocene and Quaternary fault displacement and emergence rates, and from these we estimate an average earthquake recurrence interval.

Readers less interested in geodetic measurement and analysis can refer to the summaries in the following three sections.

Deformation Preceding the Earthquake: 1926–1952

Three sources of evidence bear on deformation in the vicinity of the White Wolf fault prior to the 1952 earthquake: repeated level surveys reveal near-fault vertical deformation, repeated triangulation surveys yield high fault-crossing strain and broad-scale secular shear strain, and the pattern of seismicity indicates that these preseismic strain changes were not caused by foreshocks.

Leveling Errors

Orthometric height, the elevation of a point above the geoid or any reference equipotential surface, can be measured by spirit leveling. These measurements are accomplished by sequential sightings through a spirit level normal to the local vertical. Random leveling errors grow with the square root of distance, L, from a reference or starting bench mark. Sections are releveled if the forward- and back-run segments between each benchmark do not agree within the field rejection criteria, β. This leads to a statistically significant random error, α, for a survey of $\alpha L^{1/2}$, where $\alpha \sim \beta/3$ for normally distributed errors, while the standard deviation between two elevation differences becomes $2^{1/2}$ times larger than for a single survey [*Heiskanen and Moritz*, 1967]. For levels performed from 1956 to 1974, $\alpha = 1.0$ mm/km$^{1/2}$ (for first-order class I levels; *Federal Geodetic Control Committee* [1974], *Vaníček et al.* [1980, p. 507]).

An analysis of slope-dependent errors for 1100 km of southern California leveling [***Stein and Silverman***, 1980; *Stein*, 1981] demonstrates that linear correlations between geodetic tilt and topographic slope may be abundant and lead to errors of less than $(0.3 \pm 2.3) \times 10^{-5}$ times the slope or elevation difference. In the case of the level routes discussed in the text, errors should rarely exceed 45 mm on any profile presented. Since errors tend to cancel over several relevels of a route, and both fault-crossing routes have been resurveyed more than five times during the period examined, the likelihood of greater errors becomes small. The coseismic elevation changes are much larger than the slope-dependent errors and so fault models are insensitive to such uncertainties. The source of the error may be incorrectly computed or applied rod excess (the amount the rod is longer or shorter than its nominal length), or perhaps damage to some rods during use. *Strange* [1981] independently reports a systematic bias of $4–8 \times 10^{-5}$ times the height difference for levels run before 1965, caused by atmospheric refraction when sight lengths (the distance between rod and instrument) were in excess of 50 m. This means that observed elevation changes from the 1950's to the late 1960's could be on average, about 50 mm too large.

Many systematic errors can be accurately assessed by loop closure. A circuit is leveled and the difference between the initial and final measurement of the starting point elevation, the misclosure, is compared to expected random error. Individual surveys are considered separately. If for each circuit the closure is less than the expected random error, the probability of significant systematic error becomes small. Because equipotential or level surfaces need not be parallel, observed elevation (but not elevation change measured by resurvey) is path-dependent. A gravity-based geodetic correction, known as the orthometric correction, can be applied to very precise geodetic leveling to correct for the path-dependence [*Bomford*, 1971, p. 272]. To eliminate or evaluate non-tectonic bench mark displacement, regions undergoing fluid or gas withdrawal are excluded from consideration, and junction lags, the time between initial and final occupation of a bench mark, are noted. Junction lags contribute to error if any vertical movement occurs at a bench mark after initial occupation but before final occupation. Isolated subsiding bench marks are excluded from our model fitting but are retained on all profiles presented. Seismic shaking of bench marks imbedded in sediment can lead to compaction, resulting in local bench mark subsidence, and can introduce random errors larger than those errors observed during intervals between earthquakes. In general, highest confidence can be attached to elevation changes that show no bench mark to bench mark correlations with topography, and where field procedures were essentially unchanged between relevels. On all elevation change (ΔH) profiles presented, $\pm 1\sigma$ brackets that reflect random and slope-dependent errors are shown for the point farthest from the reference or fixed bench mark. The relative uncertainty of adjacent bench mark elevations is roughly the size of the dots plotted on the profiles (less than 2 mm).

Leveling Data

Two short leveling segments traversing Wheeler Ridge, a bedrock outcrop at the site of 1952 epicenter oriented normal to the White Wolf fault strike, were leveled in 1926, 1942, and 1947 (route location, Figure 2*a*). We know of no other bedrock relevels in the vicinity of the White Wolf fault after 1926. Between 1942 and 1947 the lines crossing Wheeler Ridge tilted 4–17 μrad down to the south (Figure 3). The northern extent of the tilt cannot be evaluated because fluid, gas, and water withdrawal in the southern San Joaquin Valley (documented by *Lofgren* [1975]) restrict usage of levels to consolidated Tertiary sediments and granitic basement. Down-to-the-south tilts were measured over both routes. On the steep Wheeler Ridge route, the 6% grade minimizes refraction error to ± 1 μrad, because sight lengths must be short and consequently cannot change much for different surveys. Over the gently sloping sediments of the adjacent route, the small topographic height difference, 65 m, limits rod error to ± 1 μrad. The

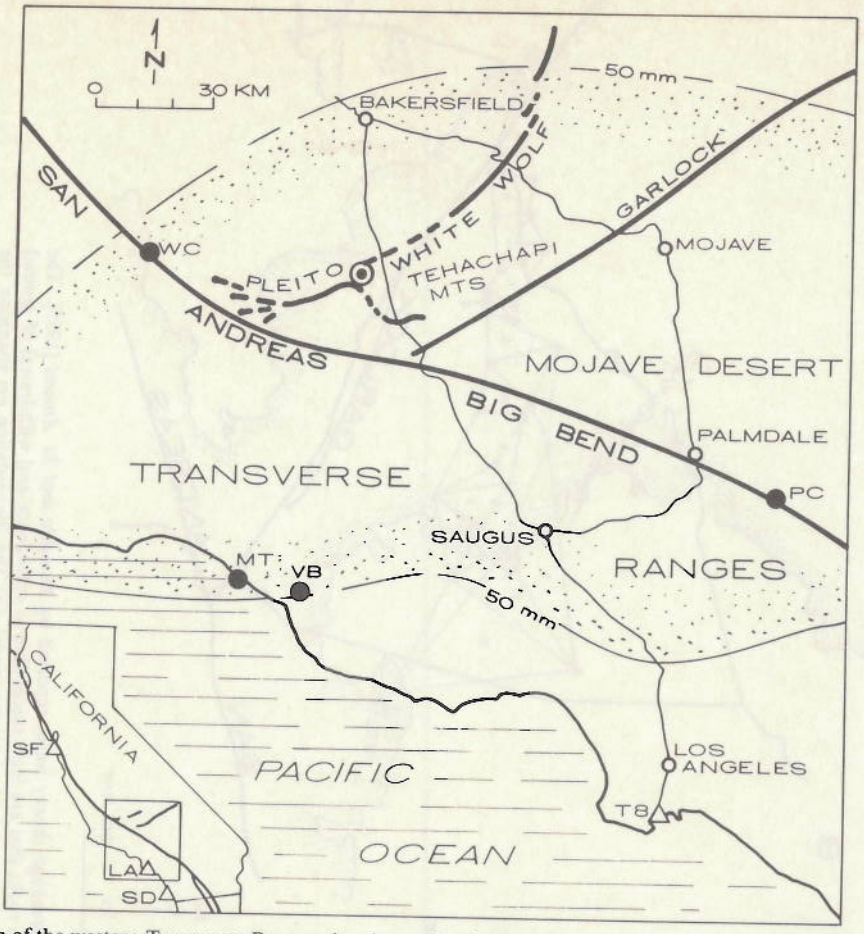

Fig. 1. Map of the western Transverse Ranges showing major faults, and the 50 mm envelope of the 1959–1974 southern California uplift [from *Castle*, 1978]. Also shown is the 450-km leveling circuit (thin line), the site of *Yeats'* [1977] determination of Quaternary uplift rate (VB), the site where *Wehmiller et al.* [1977] measured the rate of marine terrace emergence (MT), the sites of the displacement rate indicators on the San Andreas fault at Wallace Creek (WC) and Pallett Creek (PC), the epicenter of the July 21, 1952, earthquake (target), the Tidal 8 bench mark at San Pedro (T8), and the San Francisco and San Diego tidal gauges (inset).

1947–1942 tilts depart significantly from the 10 coseismic and post-seismic relevels of these two routes (Figure 3*b*), suggesting that the tilts are not simply the product of weak near-fault rocks, such as gouge.

Triangulation

Angle changes between consecutive surveys of the Kern County triangulation net, shown in Figure 2*b*, were analyzed by *Dunbar* [1977] and *Dunbar et al.* [1980]. Using the method of *Frank* [1966], two independent shear strains can be obtained without holding any line azimuth or length fixed. These shear strains are defined by the relations $\gamma_1 = e_{11} - e_{22}$ and $\gamma_2 = 2e_{12}$, for axes oriented north (subscript 2) and east (subscript 1) (see Table 1). γ_1, γ_2, and their standard deviations can be calculated by fitting a uniform strain field to the angle changes in a given polygon by the least-squares method [*Savage and Burford*, 1970]. This requires that strain be uniform in a polygon with more than three sides. Certainly strain will not be uniform within the 20 to 200 km^2 polygons in the presence of fault slip, except at large distances from the slip surface. Together with survey measurement errors, the non-uniformity of the strain field will be evident in the strain standard deviations, which are shown in Figure 4. The results plotted in Figures 4 and 8 have been taken from *Dunbar et al* [1980] except that standard deviations for triangular figures have been enlarged since non-uniformity of strain cannot be measured there.

Left lateral shear parallel to but not across the White Wolf fault (γ_1), displays no significant variation in strain with distance from the fault. The 1952$^-$ survey was performed from Novemer 1951 to May 1952, two months before the quake. The mean value of γ_1 ($\bar{\gamma}_1$) during 1932–1952 is 7 ± 2 μstrain, a rate of 0.35 ± 0.1 μstrain/yr. $\bar{\gamma}_2 = 0.2 \pm 2.0$ μstrain and does not differ significantly from zero. If the mean shear strain rate during 1932–1952 was roughly constant, then it is similar in magnitude to that found elsewhere in California, such as on nearby segments of the San Andreas fault [*Thatcher*, 1979], and shows no sustained increase prior to the Kern County shock.

The preseismic tilt observed near the epicentral region during 1942–1947 appears to have been accompanied by a near-fault horizontal strain anomaly in the central fault reach. The left-lateral shear strain rate, $\dot{\gamma}_1$, across the fault, is twice as high as the shear strain rate averaged over the entire net for that epoch, and differs significantly from the mean at the 2σ level of confidence. The high rate of strain for polygon *c* may record a temporal excursion sometime during the 20 years before the earthquake. While strains may be commonly higher at the White Wolf and Garlock faults in the presence of either fault creep or weaker rocks, the preseismic value of *c* is twice the

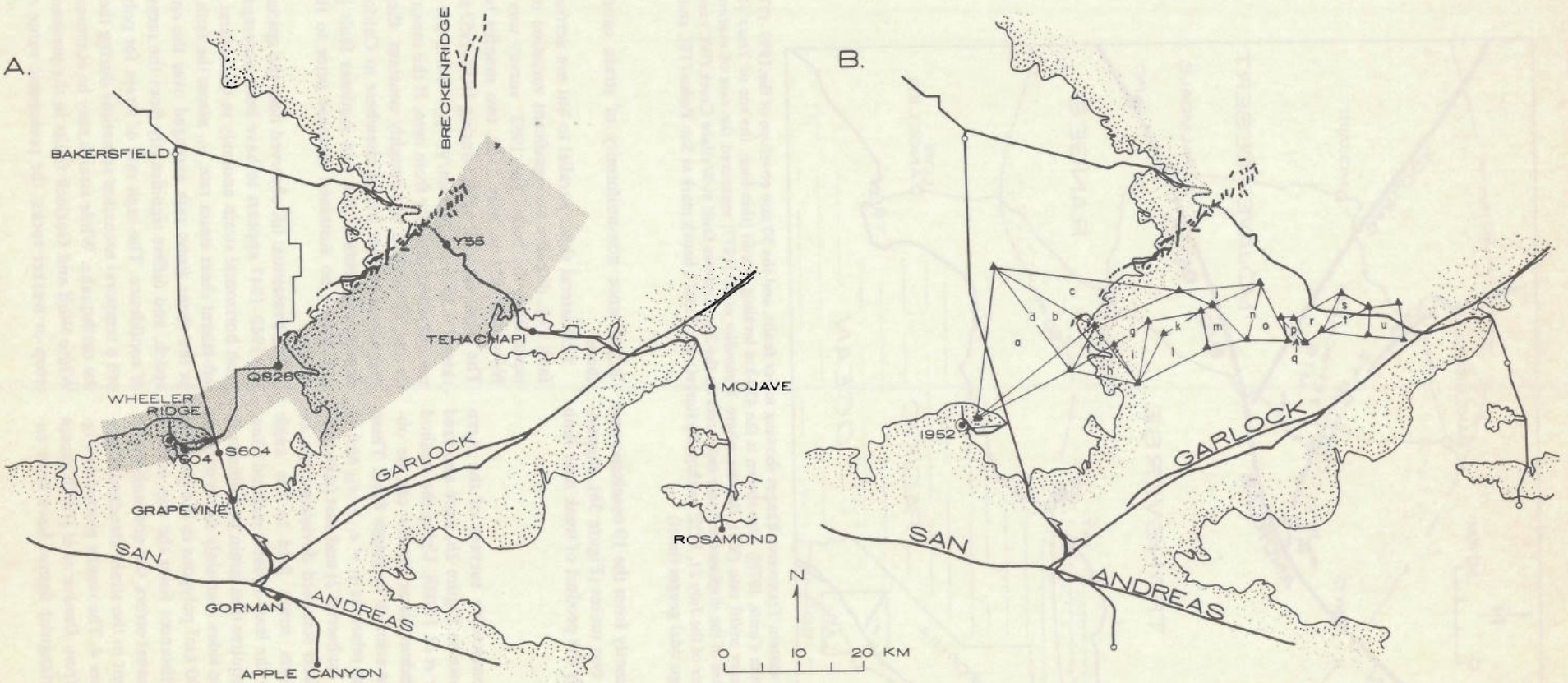

Fig. 2. (*a*) Leveling routes (light lines), and the 1952 ground breakage (heavy lines) reported by *Buwalda and St. Amand* [1955]. The speckled region includes consolidated Tertiary deposits and granitic rocks that are least susceptible to subsidence and withdrawal of ground water. The shaded region represents the surface projection of the fault approximated by the model. (*b*) The triangulation net spanning the White Wolf and Garlock faults. The letters correspond to the braced strain polygons. Shear strain for every other polygon is determined independently.

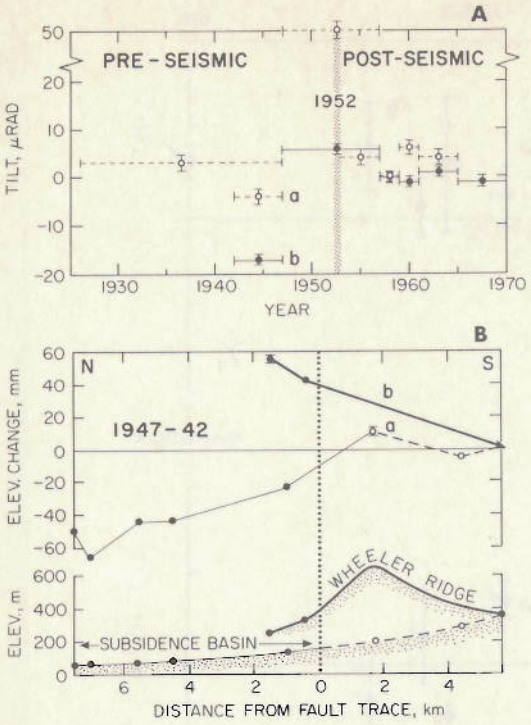

Fig. 3. (*a*) Tilts over the segments shown in Figure 3*b* for the epoch 1926–1970. The 1947–1942 tilts depart significantly from the coseismic and postseismic tilts. Error bars represent 1σ for the random and slope-dependent errors. (*b*) Profiles of leveling segments in the epicentral region of the White Wolf fault. North of the fault, pumping of water causes subsidence that obscures tectonic tilts.

magnitude of its post-seismic value. This suggests that the strain reflects a temporal anomaly and is not simply the result of weak rocks.

Seismicity

Ishida and Kanamori [1980] found that much of the fault plane of the Kern County earthquake had been seismically quiet for nearly 15 years before the main shock. In the immediate vicinity of the epicenter, activity had been very high during the same period (Figure 5*b*). However, the summed moment of all shocks between 1942 and 1947 near the epicenter, or 1932–1952$^-$ at the central fault reach, is much too small to have caused the measured tilt and shear strain anomalies.

Earthquakes before the installation of the southern California seismic network in 1932 have been compiled by *Toppozada et al.* [1978]. Although the locations and assignments of magnitude are less accurate, the absence of shocks on the fault plane apparently extends to 1901. A possible exception to this are the 1916 $M = 6.0$ and 5.5 earthquakes. The epicenter of the larger shock was located approximately at the intersection of the San Andreas and Garlock faults [*Branner,* 1917; *Allen et al.,* 1965]; it may have occurred on the San Andreas fault.

Summary

Four to seventeen μrad tilts developed between 1942 and 1947, almost precisely at the July 21, 1952, epicenter. The rate of horizontal shear strain between 1932 and 1952$^-$ on the fault-crossing strain figure was two times higher than the average for the triangulation net, and the maximum left-lateral shear was oriented nearly parallel to the White Wolf fault. These deformations were not accompanied by significant earthquake activity. The magnitude of both preseismic observations is two to four times the secular or background signal.

Slip Configuration of the Kern County Earthquake

We investigated the 1952 earthquake to calculate the fault slip, compared the calculated slip to the aseismic deformation before and after the earthquake, and developed a recurrence rate for earthquakes with similar vertical fault slip. A good approximation to the vertical displacement field caused by the 1952 Kern County earthquake can be obtained by differencing pre-shock and post-shock surveys that are tied to a distant sea-level reference point. We then modeled vertical displacements by trial and error with an elastic dislocation model, using the aftershock zone to delimit the horizontal length of the faulted slip surface. On the basis of constraints imposed by the horizontal shear strains from triangulation, we solved for the coseismic slip vectors and the shape and orientation of the slip surfaces that fit the vertical displacements. Greater emphasis was placed on modeling vertical displacements because leveling observations are more abundant, more accurate, and have a higher spatial resolution than horizontal strains reduced from triangulation. Independent geophysical and geological evidence provided supplementary support for the non-uniform fault geometry deduced from modeling. Readers less concerned with modeling procedure should skip to the section entitled 'model fault geometry.'

Control Point for Coseismic Elevation Changes

To evaluate coeseismic elevation change, rather than merely tilt, levels must be tied to an approximately invariant reference or control point. If the surface containing the point can be assumed to pass through mean sea level (msl) at San Pedro in 1926 (T8 in Figure 1), and remain unchanged through 1974, then two approaches to establish an invariant control point become feasible:

1. Relative sea level at Tidal 8 in San Pedro has risen at an average rate of 0.5 ± 0.2 mm/yr over the interval 1924–1973. We subtract the eustatic sea-level rise of 1.5 ± 0.2 mm/yr [*Hicks and Crosby,* 1975] from this, leaving a residual non-eustatic rate of uplift at Tidal 8 of 1.0 ± 0.4 mm/yr. (*Wood and Elliot* [1979] perform a similar set of calculations for the period 1853–1978; see their Figure 5.)

2. If either San Diego or San Francisco (the two nearest continuously recording tide gauge stations, shown in Figure 1, inset) have remained tectonically stable, then differencing msl at San Pedro with msl at San Diego or San Francisco should yield the same rate at Tidal 8, free of any assumptions about the eustatic sea level trend. In fact, Tidal 8 has risen with respect to both San Diego (1.1 ± 0.3 mm/yr) and San Francisco (1.3 ± 0.5 mm/yr) at a similar rate. The standard deviation of the trend for the T8–San Diego difference is smaller because the tide gauges are only 150 km apart and share nearly equivalent meteorological and oceanographic regimes. The convergence of the two methods on an uplift rate of 1.0 ± 0.24

TABLE 1. Horizontal Shear Strains

Tensor Strain Components	Resolved on Fault of Type	
	Right Latitude	Left Latitude
$\gamma_1 = e_{11} - e_{22}$	N45°W	N45°E
$\gamma_2 = e_{12} + e_{21}$	E-W	N-S

Surface shear strains computed from triangulation data. No dilatational or rotational component of the strain field is retrieved; no line azimuth or length is assumed invariant. Shear strain within every other polygon is determined independently.

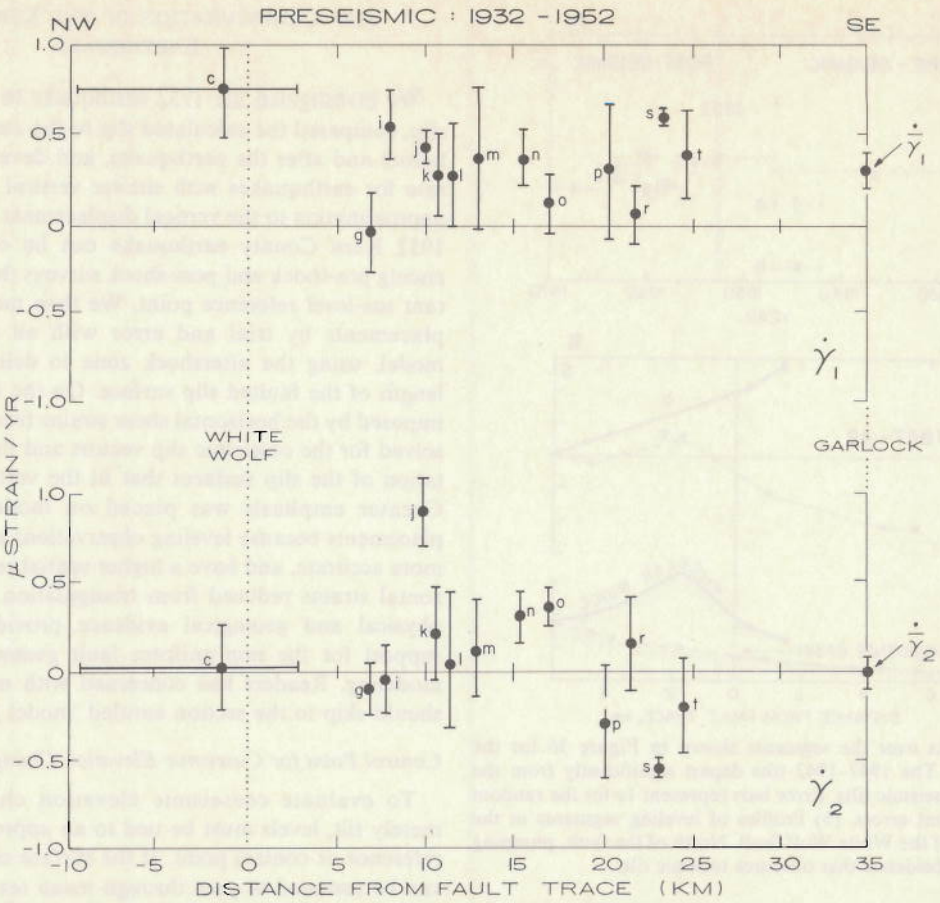

Fig. 4. Preseismic changes in the rate of horizontal shear strain from triangulation, calculated according to Table 2. $\dot{\bar{\gamma}}$ is the mean value for each component. Letters correspond to strain polygons of Figure 2*b*. Polygons a, b, e, f, and h were not surveyed until 1952. The extent of strain triangle *c* normal to the White Wolf fault is shown with horizontal brackets.

mm/yr suggests that San Diego and San Francisco remained tectonically stable since tide gauges were installed, and were not affected by the southern California uplift. The historical record of tectonic quiesence at San Diego is supported by uplift rates of 0.16 ± 0.06 mm/yr and 0.23 ± 0.05 mm/yr there during the past 125,000 and 80,000 years, respectively; these are among the lowest rates measured on the California coastline [*Wehmiller et al.*, 1977]. Mean sea level ±20 mm at San Diego can therefore be adopted as the invariant control point for all southern California leveling tied to San Pedro in 1926 and 1953.

Elevations and their associated random error can be extended from the tidal gauge at San Pedro to the White Wolf region as long as neither the 1926 nor the 1953/1955 survey shows large systematic errors. The 1926 circuit misclosure of 25.8 mm + 12.2 mm orthometric correction yields an error of 38 mm (the route is shown in Figure 1). This error is within one standard deviation of the random error for the 450-km circuit at 1926 standards and amounts to only slightly more than 1σ compared to current leveling standards. The 1953/1955 circuit incorporates two large junction lags, each of about two years duration. Fortunately, these occur more than 75 km from the White Wolf fault. The misclosure and orthometric correction yield 24.4 + 12.2 mm = 36.6 mm, slightly greater than 1σ by 1953 standards. The random error at Bakersfield, the point farthest from the reference station, becomes 48 mm (see Figure 2). Both circuits conform to standard first order leveling specifications and are therefore suitable for evaluation of coseismic elevation changes.

Model Fault Geometry

Once rough values of the dip slip displacements on the fault were fixed from separate two-dimensional elastic dislocation models of the elevation differences along the N-S and NW-SE level routes, the 75 km fault length was divided into three 25-km-long segments with variable orientation, slip, upper and lower fault extent, and dip. We segmented the fault into three planes because we found that the displacements cannot be satisfied by a single fault plane, and we employ three sets of fault-crossing levels in the modeling process (Figure 2*a*).

A program employing the closed form analytical expressions of *Mansinha and Smylie* [1971] to accommodate multiple slip surfaces with displacements resolved on the free surface was used to model observed displacement and strains. The shear strains γ_1 and γ_2 are computed by a finite differencing scheme that yields spatially averaged strains for 20 km^2 squares. Comparison with *Dunbar*'s [1977] exact computation of γ_1 and γ_2 for each polygon in the net shows that the approximation is accurate to within ±5% except where strain variation within a polygon is large, in which case errors could be larger.

From the epicentral region toward the northeast, the fault model displays decreasing reverse and left-lateral slip, decreasing upper and lower fault depth, and shallowing dip. Beneath the epicenter, the slip surface dips steeply at 75°, displays 3.5 m of left-lateral reverse slip, and extends to a depth between 20 and 27 km. Near Caliente in the northeast, the fault dips 20°, shows about a meter of largely left-lateral slip, and extends to a depth of only 10 km. The surface projection

of the fault model that provides the best fit to all data is plotted in Figure 2*a*, and an isometric diagram of the best-fit model is shown in Figure 6. The fault parameters are listed in Table 2.

The quality of the model fit (and the model for a 19 km epicentral fault depth) to the elevation differences can be judged from the profiles in Figure 7. On the N-S Bakersfield-Apple Canyon profile, all observations lie well within 1σ of the model profile. Surveys performed prior to and following the earthquake at different times are employed to increase the total number of resurveyed bench marks near the fault. The substitution of the 1947 survey from BM K54 (km +12.5) north to S54 (km −10, not shown on the profile) allows the inclusion of seven critical near-fault BMs and shortens the coseismic epoch in this region from 27 to 6 years. To assess the error caused by the substitution, we close the 1926 circuit with the 23-km 1947 segment substituted where we have used it in the profile. This results in a misclosure 20 mm larger than that for 1926 leveling alone. This means that the near-fault BMs

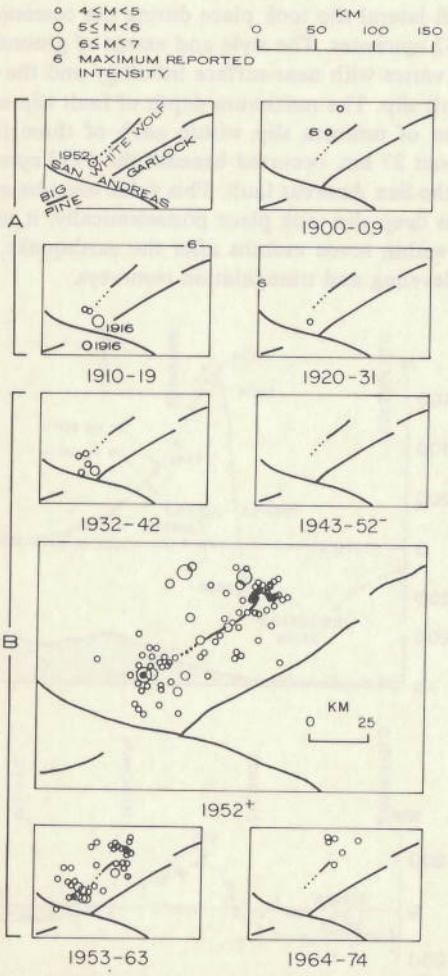

Fig. 5. Seismicity of the White Wolf region, 1900–1974. (*a*) Earthquakes during these three decades have been located and assigned magnitudes from reported intensity distribution by *Toppozada et al.* [1978]. Since the region was sparsely populated until around 1940, it is possible both that some $4 < M < 5$ shocks prior to 1932 may not have been recorded, and that many epicenters may have been mislocated by as much as 50 km (T. R. Toppozada, oral communication, 1978). (*b*) Earthquakes from 1932–1952$^+$ were relocated by *Ishida and Kanamori* [1980], and shocks from 1953 to 1974 have been located within the California Institute of Technology southern California net [*Hileman et al.*, 1973].

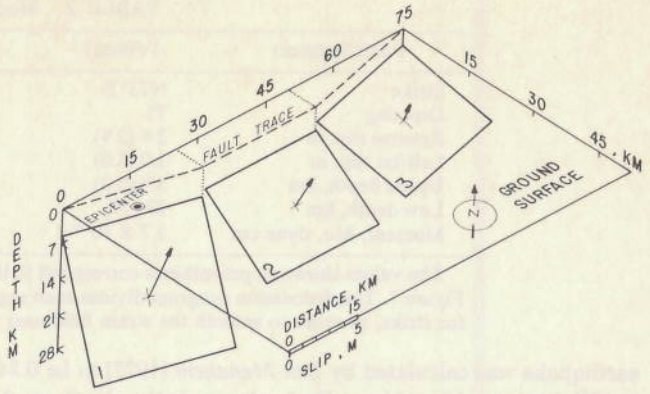

Fig. 6. Isometric diagram of modeled fault with curved surface trace approximated by three planar surfaces. Slip vectors are drawn on each fault plane. Note increasingly shallow fault burial below the ground surface from segments 1 to 3. The 1952 epicenter is shown by a target.

can be included in the coseismic elevation change profile, with an additional ±20 mm error in the standard deviations of those BMs. The same procedure is used for the 1926–1957 and 1947–1957 segments.

The NW-SE Bakersfield-Rosamond level line exhibits considerably greater noise; secondary surface faulting and contamination from Edison oilfield may obscure the coseismic signal in the northwest. After imposing a uniform correction of −50 mm (to be discussed), all of the observations on the hanging-wall block fall within 1σ. The 1952–1953 coseismic strain changes deduced by *Dunbar et al.* [1980] are presented in Figure 8. About 50% of observations lie within 2σ for γ_1, with 80% of observations within 2σ for γ_2. While greater emphasis has been placed on satisfying the more accurate leveling observations, integration of the triangulation net with leveling constrained the model fault to have a curved trace, which we have approximated with three straight segments. This results in a fault strike continuous with the N70°E striking Pleito fault to the southwest, and the N30°E striking Breckenridge fault to the northeast. Both adjacent faults extend into the 1952 aftershock zone. Horizontal shear strains also confirm the presence of a significant left-lateral slip component that decays to the northeast, visible in Figure 6.

The nearly uniform −50 mm depression in elevation change through Mojave, Rosamond, and persisting nearly to Palmdale, 40 km to the south (Figure 7*b*), presents a problem in fault modeling: Slip confined to faults within or near the 1952 aftershock zone fails to produce such a pronounced regional elevation drop. Nor do horizontal shear strains substantiate such large regional displacement; as close as 30 km from the northeast fault segment, strains become negligible. Subsidence caused by water withdrawal or sediment compaction can be eliminated because the line traverses granitic bedrock between Techachapi and Mojave and just north of Rosamond, as evident in Figure 2*a*. The 50 mm ΔH may result from widespread pre-seismic changes or slope-dependent errors, and is within the range found by *Stein* [1981] and *Strange* [1981]. The control point for the model has been adjusted −50 mm in Figure 7*b* to isolate presumed coseismic elevation changes, although we cannot be certain that it is in fact an error.

Independent assessment of the model fit can be made by comparison between modeled and measured earthquake parameters. The seismic moment, M_0, of the July 21, 1952,

TABLE 2. Model Fault Parameters

Fault Segment	1 (West)	2 (Central)	3 (East)	Net
Strike	N73°E	N58°E	N43°E	
Dip, deg	75	35	20	
Reverse slip, m	2.4 (2.9)	1.0	0.4	1.3
Left-lat slip, m	2.0 (2.0)	2.0	1.0	1.7
Upper depth, km	5.0 (5.0)	3.5	2.0	
Low depth, km	27 (19)	15	10	
Moment, Mo, dyne cm	5.7×10^{26}	3.3×10^{26}	1.6×10^{26}	1.1×10^{27}

The values shown in parentheses correspond to the 19 km deep fault model shown as a dashed curve in Figure 7. The dislocation program divides each segment into two planes with identical parameters except for strike, in order to smooth the strain field near segment junctions.

earthquake was calculated by *Ben-Menahem* [1977] to be 0.84×10^{27} dyne cm. Here $M_0 = \mu \sum uA$, where μ is the elastic modulus of rigidity, assumed to be 3×10^{11} dyne/cm^2, u is the slip magnitude, and A is the slip surface area. The geodetic model yields $M_o = 1.0 \times 10^{27}$, conforming within observational error to the moment measured from seismic waves. The fault-plane solution of the July 21, 1952, earthquake calculated by *Gutenberg* [1955] using P wave first motion and S wave polarizations yields a strike of N50°E and dip of 63°S, with the dip slip component about 1.4 times larger than the left lateral slip. For the epicentral fault segment 1, the model shows a strike of about N65°E, a dip of 75°S, and dip slip a factor of 1.2 more than strike slip, providing satisfactory agreement.

Surface Rupture

Whereas the gross pattern of maximum observed surface rupture is compatible with the modeled fault slip, the local variation of surface offset is not supported by geodetic measurement (see Figure 9). Where a 5– to 7–km thick sediment cover mantles the basement rocks beneath the 1952 epicenter, little or no surface breakage was reported. To the northeast along the front of Bear Mountain (km 20–50 in Figure 9), ground breakage was confined mainly to debris aprons and alluvial fan deposits that displayed many different surface slip patterns. Many traces were complicated by landsliding and slumping [*Buwalda and St. Amand*, 1955, p. 43]. Cuts developed during repair and revision of Southern Pacific Railroad tunnels revealed bedrock fractures dipping 30°–45° beneath the eastern flank of Bear Mountain. Along this reach of the fault, no more than a 1 km thick layer of sediments overlies the basement rocks; surface rupture occupies a band 2–3 km wide, and the profile of coseismic elevation change shows about 100 mm more noise than near the epicenter (compare Figures 7*a* and 7*b*).

The rupture zone may become more diffuse or the slip surface may splay within the sediments near the ground surface, creating secondary thrusts. *Jungels and Frazier* [1973] found that the best fit to elevation changes associated with the 1971 M6.4 San Fernando earthquake was made by splaying the rupture zone into three near-surface (0–2 km depth) faults, or imposing plastic deformation in this zone. Finite element modeling by *Jungels and Frazier* [1973] of an alluvial basin by modulus reduction in a layered half space to account for lithologic contrasts within the upper few kilometers did not, however, change the calculated vertical displacement from that of a homogeneous half space by more than about 10% [see *Jungels and Frazier*, 1973, Figure 6]. Therefore, geodetic modeling of earthquake displacements is relatively insensitive to near-surface lithology; an homogeneous elastic half space appears a simple and adequate approximation. The pattern of ground offset, on the other hand, appears highly dependent on the depth and location of faulting and may not accurately record the buried slip and its variation along the fault strike.

Summary

Decreasing fault depth, slip, and dip away from the 1952 epicenter toward the northeast satisfies the geodetic record and appears consistent with the seismic moment and fault-plane solution, as well as geologic constraints. About 3 m of reverse left-lateral slip took place during the coseismic epoch at the 1952 epicenter. The style and extent of ground rupture evidently varies with near-surface lithology and the depth of planar fault slip. The maximum depth of fault slip under the assumption of uniform slip within each of three fault segments, about 27 km, occurred beneath the 1952 epicenter, 30 km from the San Andreas fault. This value must be at least 20 km. If this deep slip took place postseismically, it must have occurred within seven months after the earthquake, prior to the 1953 leveling and triangulation resurveys.

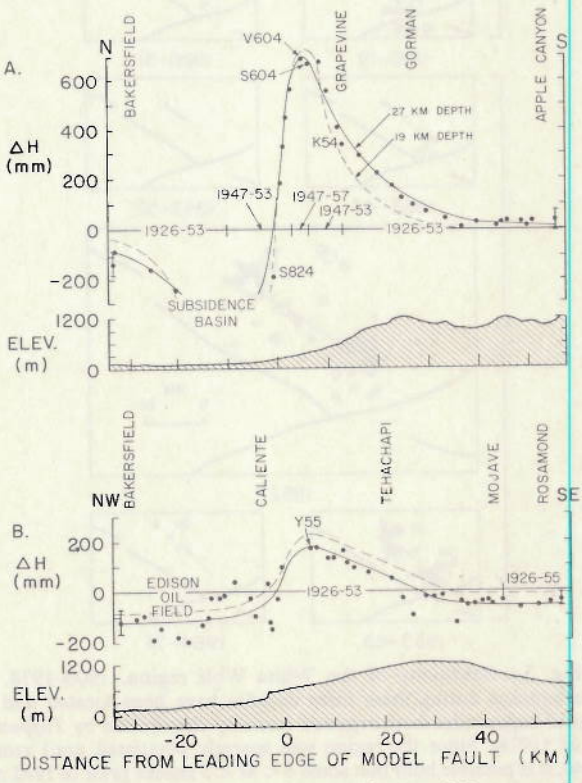

Fig. 7. Coseismic elevation changes (dots) and fit to an elastic dislocation model (curves) with route topography shown. (*a*) The dashed line shows the best fit for a fault that extends to 19 km beneath the epicenter. (*b*) The control point for the model curve has been shifted −50 mm from the dashed to the solid curve for reasons discussed in the text.

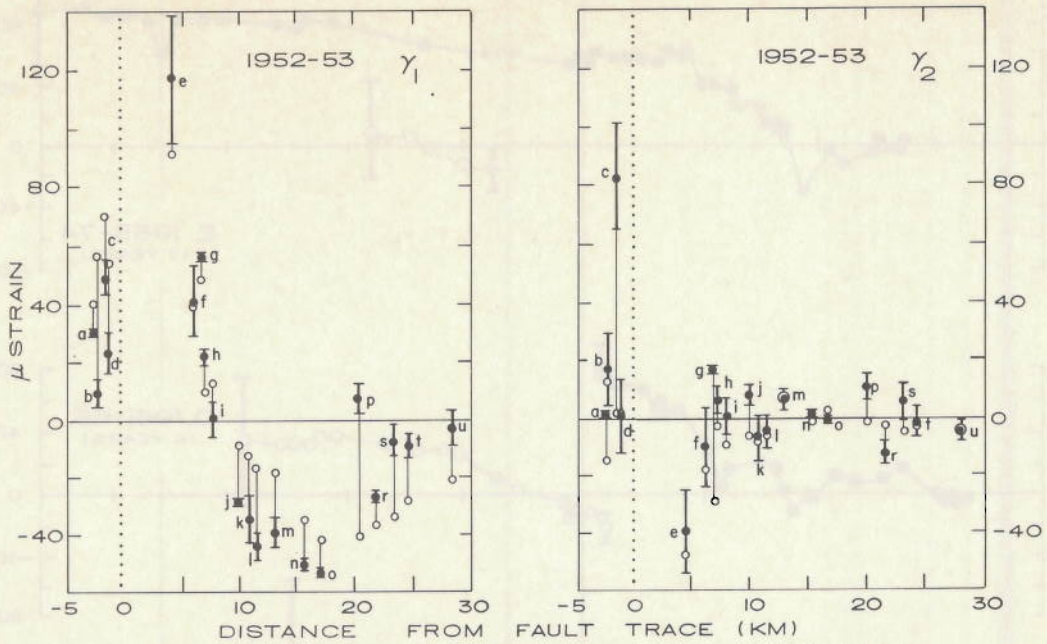

Fig. 8. Coseismic shear strain changes (dots with error bars) accompanied by model fit (circles). Letters correspond to strain polygons of Figure 2*b*.

DEFORMATION AFTER THE EARTHQUAKE: 1952⁺–1974

Leveling

During the post-seismic period, we hold Bakersfield (BM F55/P825) fixed because ties to Tidal 8 are infrequent. All elevation changes are relative to this point.

From seven months to seven years after the 1952 earthquake, a nearly uniform 27 ± 11 mm elevation gain developed on the two lines that traverse the 1952–1959 zone of aftershocks. No offset can be seen across the fault in either fault reach (see Figure 10*a*, dots; Figure 10*b*, circles).

Seven years after the earthquake, the rate of deformation within the aftershock zone dramatically increased, unaccompanied by surface offset at the fault trace (Figures 10*c*–10*e*). By 1970, uplift reached 120–170 mm near the fault. This represents almost 100% of the coseismic elevation change in the northeast, and about 25–50% of the uplift at the same BMs near the epicenter. The post-seismic elevation changes extend

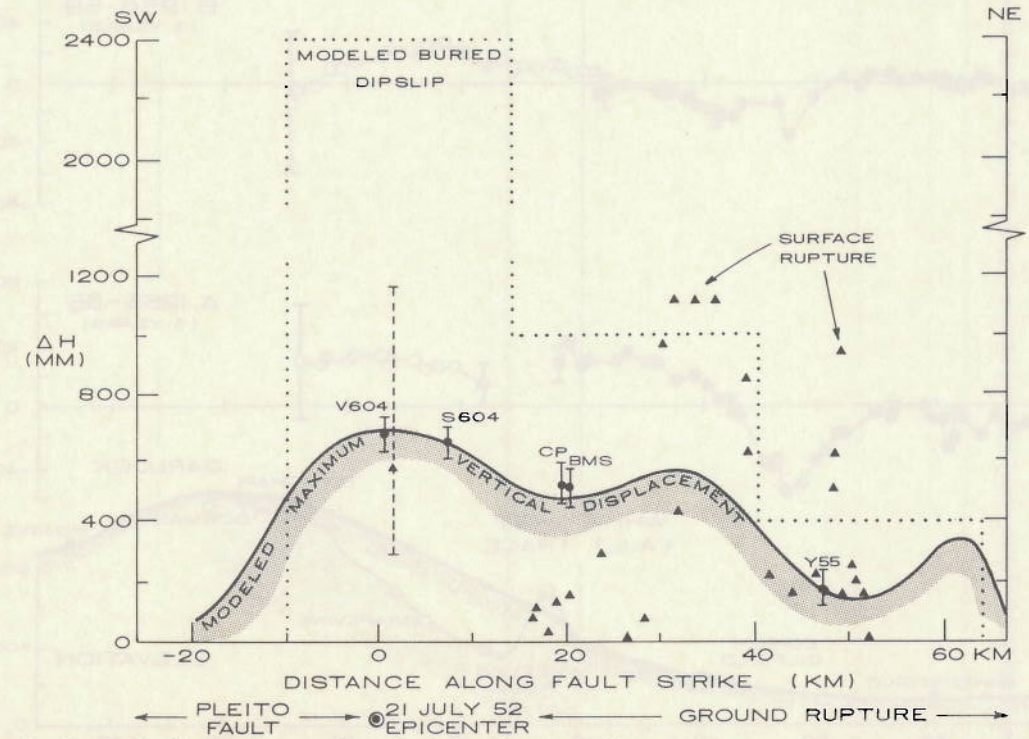

Fig. 9. Coseismic elevation changes along the fault strike (dots with error bars), model fit (curve), and dip-slip component of ground rupture (triangles) from *Buwalda and St. Amand* [1955]. The 1–10 km scale variation in surface offset is not apparent in surface deformation or modeled fault slip. Bench marks on Commanche Point are centrally located on the fault.

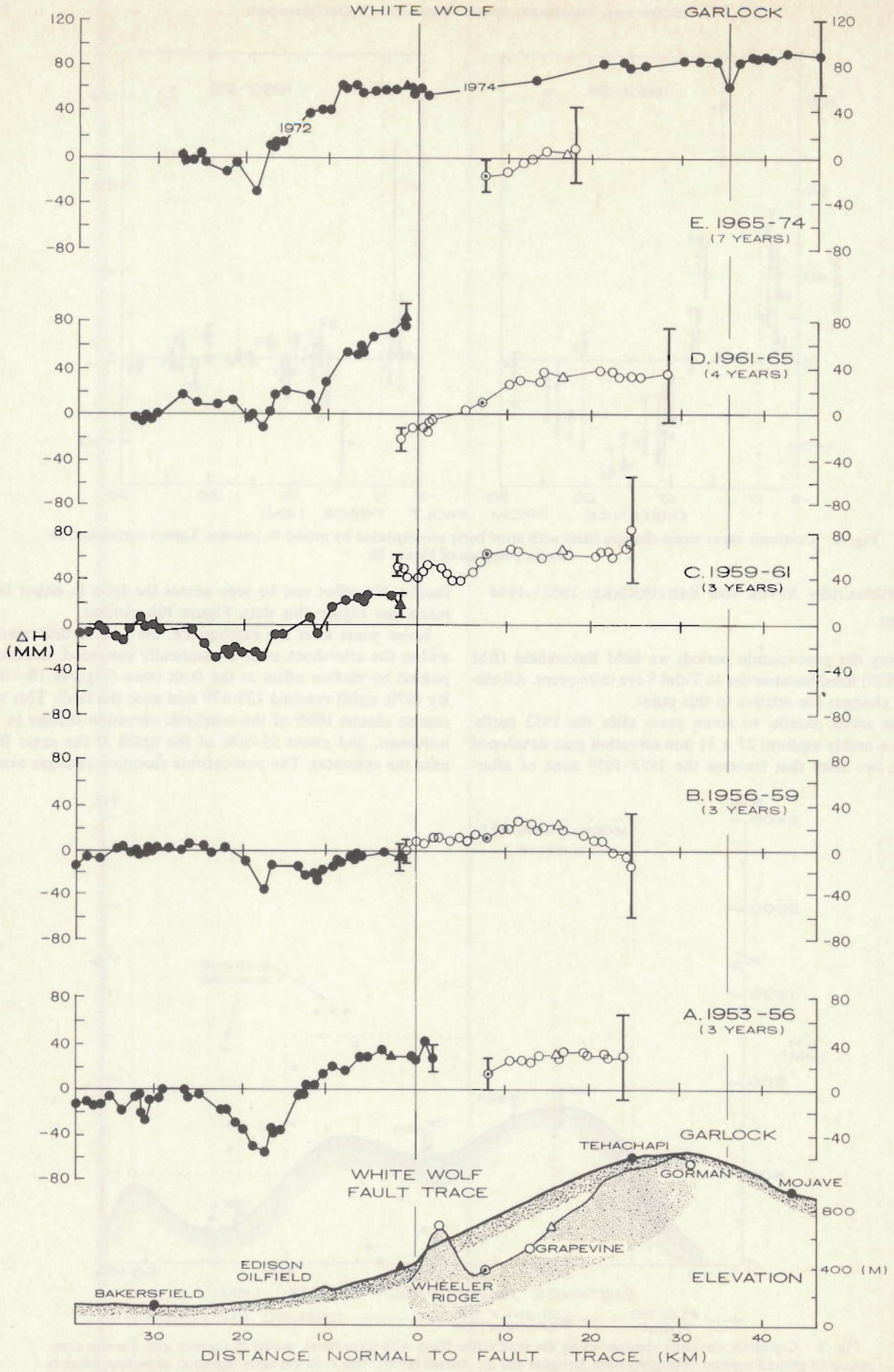

Fig. 10. Sequential profiles of post-seismic elevation change from the NW-SE Bakersfield-Mojave route (dots) and the N-S Wheeler Ridge–Gorman route (circles), both projected onto an azimuth normal to the White Wolf fault. For route locations, see Figure 2*a*. Bakersfield is held fixed for these reconstructions. The second order 1970 survey differences are not shown.

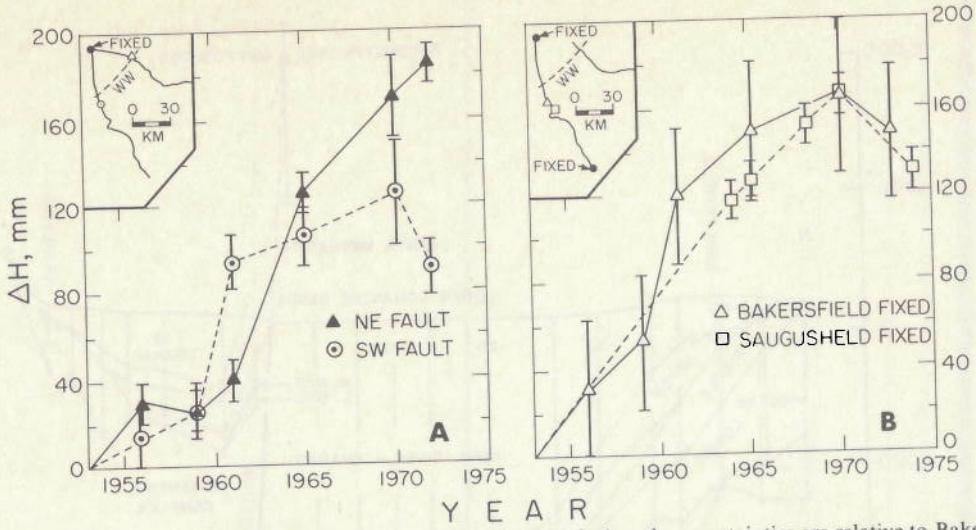

Fig. 11. Displacement as a function of time. (*a*) Comparison of the fault ends; uncertainties are relative to Bakersfield. These BM's (target, triangle) are shown in Figure 10. (*b*) Comparison of adjacent BM's, D367 tied to Bakersfield, and E367 tied to Saugus. Slope-dependent error has been removed from E367 as in *Stein* [1981]; its brackets reflect the error of adjustment.

outside of the 1952 aftershock zone, about 50 km SE of the fault and 65 km SSE of the fault, to within 10 km of Saugus (Figure 1; see *Stein* [1981]).

Uplift after 1956 commenced in the vicinity of the 1952 epicenter and appears to have propagated to the northeast. By the time the rate of uplift slowed near the epicenter (Figure 11*a*, circles), it began to accelerate in the northeast fault region (Figure 11*a*, triangles). Comparing the successive periods 1956–1961 and 1961–1970, the epicentral fault region uplifted twice as fast during the first interval as during the second—about 17 mm/yr slowing to 4 mm/yr. The northeastern region displayed the opposite trend, rising at 3 mm/yr during the first interval and 15 mm/yr during the second. Throughout the postseismic interval of 1956–1972/4, aftershocks with magnitudes greater than or equal to 3 were twice as frequent at the northeast end of the fault than at the epicentral end.

Strange [1981] argues that mean sight lengths in excess of 50 m cause elevation-dependent errors produced by optical refraction. Relevels performed after 1964 were carried out with sight lengths less than 50 m, but some of those performed before this date have mean sight lengths of up to 65 m. If the refraction error accumulates, it happens when resurveys have different sight lengths. An optical refraction model suggested by *Strange* [1981] reduces the 1955–1972/4 uplift at the Garlock fault (Figure 10*e*) by 90 mm with respect to Bakersfield. For BM S55 (dark triangle, Figure 11*a*), its 180 m elevation above Bakersfield renders the maximum potential refraction error to 20 mm (error $\leq 10^{-4} \cdot \Delta H$). Refraction can have less effect on the N-S leveling route to Gorman, because the mean 3% grade limits sight lengths greater than 40 m.

Triangulation

During the first decade after the earthquake (the initial survey was carried out one to six months after the quake), the triangulation net resurvey shows a horizontal shear strain rate, $\bar{\gamma}$, about twice that observed during the preseismic interval, 0.8 ± 0.2 μstrain/yr. For the period 1953–1963, the average shear strain, $\bar{\gamma}_1$, equaled 7 ± 1 μstrain, and $\bar{\gamma}_2$ equaled 4 ± 1 μstrain. The high value of $\bar{\gamma}_1$ may result from deep left-lateral slip with a magnitude about 25% of that modeled for the earthquake, or about 0.5 m [*Dunbar*, 1977]. For both γ_1 and γ_2, the spatial strain gradients are much higher near the epicenter than toward the northeast during the decade 1953–1963. Deformation may have been concentrated near the epicenter or concentrated near the fault trace. These two possibilities cannot be rigorously distinguished because the triangulation net crosses the fault in the southwest but lies as much as 30 km from the fault trace in the northeast (see Figure 2*b*).

Summary

The region of earthquake aftershocks did not significantly uplift for seven years after the 1952 shock. It then rose 120–170 mm during 1959–1972/4, which amounts to 25–100% of the coseismic uplift. The deep epicentral slip during the coseismic epoch may have accompanied the earthquake or followed it as post-seismic creep. Post-seismic surface fault slip was absent. The rate of uplift at the epicenter was greater than elsewhere in the region of the fault during the first decade following the earthquake. The post-seismic strain rate may result from about 25% of the coseismic left-lateral slip.

GEOLOGIC DISPLACEMENT OF THE WHITE WOLF FAULT

Late Quaternary Displacement Rate and Earthquake Recurrence

To obtain an average long term displacement rate for the White Wolf fault, we have sought the most recent time stratigraphic indicator available with measurable separation across the fault. An ash unit that may have been deposited between 0.6–1.2 m.y. ago can be identified 3000 m below the surface adjacent to the White Wolf fault.

A search of the logs of 90 oil wells drilled on the footwall block of the White Wolf fault has revealed eight core descriptions of a volcanic ash penetrated 2800–3080 m below sea level (see Figure 13, inset). The youngest ash deposit identified so far elsewhere in the sediments of the southern San Joaquin Valley is the Friant Pumice Member of the Turlock Lake Formation. This was sampled 225 km north of the White Wolf fault and was found by K-Ar analysis to be 0.6 m.y. old [*Janda*, 1965]. This ash has also been identified by *Wehmiller et al.* [1977] 100 km south of the White Wolf fault in the Ventura Basin. *Davis et al.* [1977] sampled an ash at least 0.6 m.y. old only 70 km north of the fault that they correlated with the 0.7 m.y. Bishop Tuff. *Hillhouse and Cox* [1976] reported 0.7 to

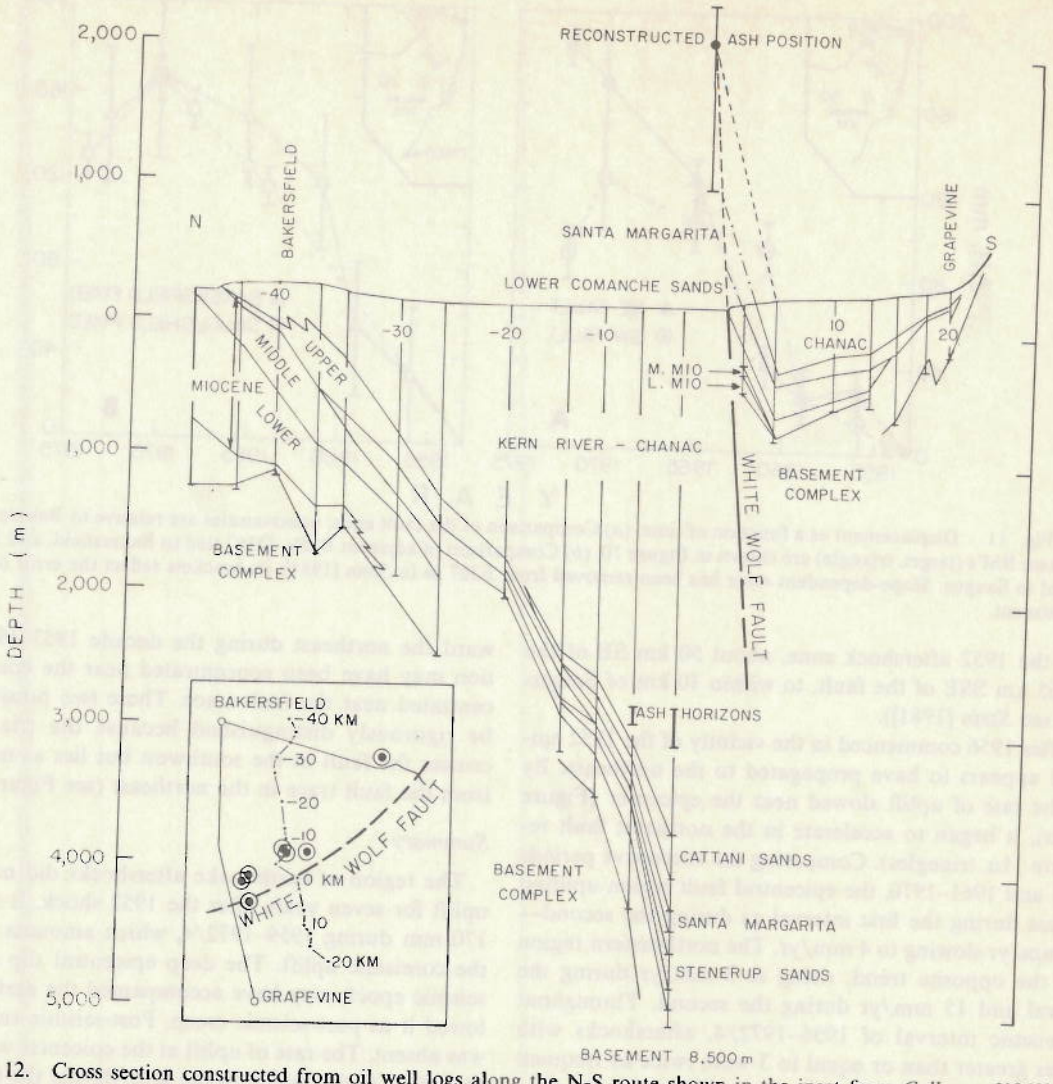

Fig. 12. Cross section constructed from oil well logs along the N-S route shown in the inset from *Callaway* [1969]. Ashes are found at a depth of about 3300 m below sea level. Note the extremely thick wedge of non-marine Quaternary sediments on the footwall (N) fault block. Distance of the wells from the fault trace are shown at sea level in kilometers. The vertical exaggeration is 12 times.

2.0 m thick ash deposits of the Bishop and a slightly younger ash, the 0.6 m.y. Pearlette 'O' from the Yellowstone caldera, that crop out 230 km east of the White Wolf fault in the eastern Mojave Desert. A 6 mm thick depsit of the 0.9 m.y. ash of Mono Glass Mountain, whose source is 750 km to the north, has been identified by *Wehmiller et al.* [1977] near Santa Barbara, 60 km to the southwest of the White Wolf fault. Finally, a 2- to 100-mm-thick deposit of the 1.2-m.y.-old Bailey ash (Pico Formation Ash of *Izett et al.* [1974]), whose probable source is either Long Valley (300 km north) or the Coso volcanic field (150 km northeast), has been found in the Ventura Basin by *Yeats* [1977]. The next older ash known is the 3.3-m.y.-old Nomlaki Tuff Member of the Tehama Formation, erupted from the Cascade Range 600 km to the north [*Sarna-Wojcicki,* 1976]. This ash can be excluded from consideration because its deposition predates the marine regression from the southern San Joaquin Valley, and the ashes are not found in association with a marine fauna. The time of deposition of the ash or ashes, then, may lie somewhere between 0.6 and 1.2 m.y. ago.

To determine the amount of fault slip that has occurred during the past 0.6–1.2 m.y., the pre-erosion position of the ash on the hanging-wall block must be reconstructed. Since the ash lies 1800 m above the 'Stenderup sand' identified by *Callaway* [1969] on the footwall block (Figure 12) and the 'lower Comanche sand,' coeval with the 'Stenderup sand,' crop out at the fault trace, we add the 1800 m to the 3300 m depth of the ash on the footwall block and estimate a maximum net vertical separation of about 5100 m. If rapid uplift and erosion of the hanging-wall block had commenced by the time ash deposition, however, the ash could have been unconformably deposited less than 1800 m above the 'Stenderup sand.' We therefore take 3600 m as the minimum net throw. This estimate provides a calculated rate of vertical displacement equal to 3–9 mm/yr for the late Quaternary.

The volcanic ash must have been deposited near or above present sea level, because it is found in a freshwater environment. It has therefore been uplifted less than 2000 m on the hanging-wall block and has subsided more than 3000 m on the footwall block to reach its present configuration. Thus more than two thirds of the vertical fault slip contributed to subsidence of the southernmost part of the San Joaquin Valley. The rate of emergence above msl (as distinct from the rate of slip) of the hanging wall block must be 1–3 mm/yr in the late Quaternary, considerably less than the historic geodetic rate, about 5–10 mm/yr.

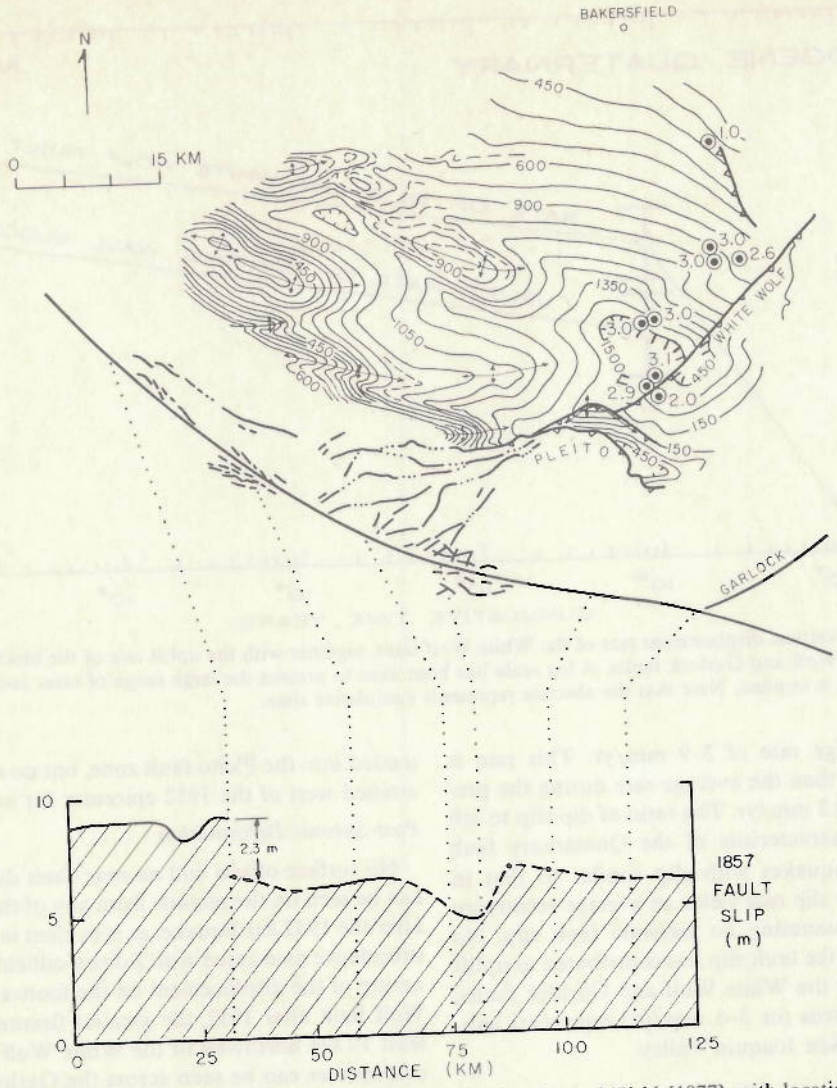

Fig. 13. (*a*) Structure contour map on the upper Miocene *N*-point chert of *Webb* [1977], with locations of ash-bearing wells (targets) and the ash depth below sea level in km. Note the great thickness of post-Miocene deposits northwest of the White Wolf fault, and the asymmetric synclinal structure of southern San Joaquin Valley. (*b*) Slip associated with the Great 1857 San Andreas earthquake by *Seih* [1978*b*] reveals about a 2 m reduction where the Pleito fault or its branches reach the San Andreas fault.

The ash-bearing wells lie within fault model segments 1 and 2; the average earthquake dip-slip for this region is about 1.5 m (Table 2). For earthquakes with vertical displacements similar to that of the 1952 shock, a recurrence interval of roughly 170 to 450 years results. The range for the recurrence interval may be underestimated if permanent aseismic slip accounts for a significant portion of the observed vertical displacement. The recurrence rate is similar to the 160 yr average recurrence interval for large earthquakes on the San Andreas fault at Pallett Creek 65 km to the southeast (PC in Figure 1) and the 250-yr maximum average recurrence interval for great earthquakes along the San Andreas at Wallace Creek (WC in Figure 1), 100 km to the northeast [*Sieh*, 1978*a*].

Displacement Rate Since the Upper Miocene

To determine if the rate of displacement was different on the White Wolf fault before the Quaternary, the vertical offset of a time-stratigraphic horizon older than 1.2 m.y. must be sought. A laterally extensive upper Miocene chert produces a characteristic electric log signature, known as the *N* point, that can be correlated over much of the southern San Joaquin Valley. A structure contour map on the *N* point that has been extrapolated by *Webb* [1977] to the Santa Margarita Formation near the White Wolf fault, is presented in Figure 13. At model segment 2, the left-lateral offset as well as the vertical separation on the Santa Margarita is about 5000 m (see Figure 12). The relative components of strike slip and dip slip deduced from the 1952 earthquake, from 1.2:1 to 0.5:1, may therefore be characteristic of the cumulative geologic displacement. Although the chert has not been precisely dated, it lies between upper Mohnian and Delmontian horizons, between 6 and 10 m.y. B.P., while the Santa Margarita Formation is of middle-Miocene age, 15–20 m.y. [*Webb*, 1977]. The average rate of fault slip between deposition of these units and the ash is 0.1 to 0.2 mm/yr, a rate almost two orders of magnitude less than that since the deposition of the ash. Hence, the current pattern of thrust and left-lateral slip on the White Wolf fault must have begun or greatly accelerated some time during the late Quaternary.

Summary

A vertical separation of 3600–5100 m may have accumulated across the White Wolf fault during the past 0.6–1.2

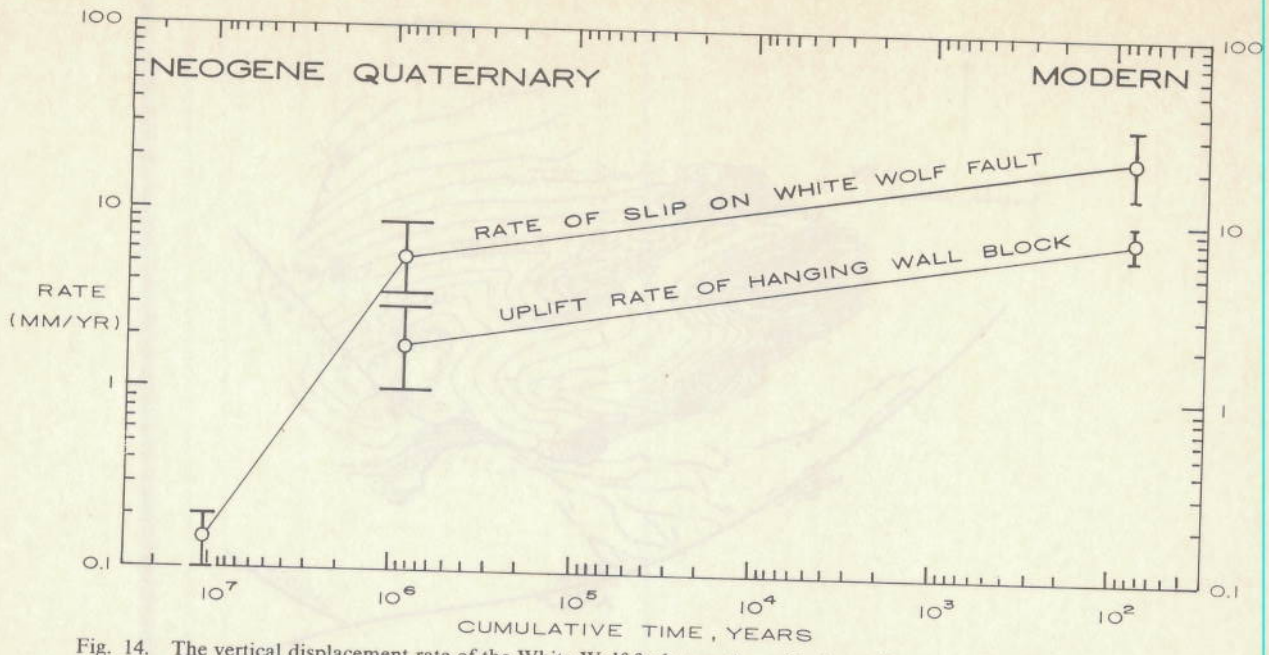

Fig. 14. The vertical displacement rate of the White Wolf fault, together with the uplift rate of the block that lies between the White Wolf and Garlock faults. A log scale has been used to present the large range of rates and time; no exponential process is implied. Note that the abscissa represents cumulative time.

m.y., yielding an average rate of 3–9 mm/yr. This rate is about forty times faster than the average rate during the preceding 10–20 m.y., 0.1–0.2 mm/yr. The ratio of dip slip to left slip in 1952 appears characteristic of the Quaternary fault displacement. For earthquakes with slip similar to that in 1952, the late Quaternary slip rate yields an average recurrence period of 170–450 yr, assuming no aseismic fault slip. No greater than one third of the fault slip has contributed to uplift of the block bounded by the White Wolf and Garlock faults, and no less than two thirds (or 3–6 mm/yr) represents subsidence of the southern San Joaquin Valley.

CONCLUSIONS

Preseismic and Coseismic Deformation

The leveling and triangulation observations, while limited in areal coverage, were ideally located and timed to record any preseismic tilts and shear strains. The relevels span the period 5–10 yr before the main shock, while triangulation covers the 0.2–20 yr period before the earthquake. Both measurements display near-fault signals that are about two to four times larger than the secular or post-seismic deformation recorded there. What is most remarkable is the absence of a larger signal; perhaps only very precise near-fault observations before moderate or larger earthquakes will reveal significant changes in displacement or strain rate.

The coseismic rupture was not at all uniform across the fault, with deep, mostly reverse slip beneath the epicenter, and shallow lateral slip to the northeast. The net slip was three times greater in the epicentral region than elsewhere along the fault (Table 2). In order to satisfy the coseismic measurements obtained from both leveling and triangulation, the White Wolf fault trace must be curved. The fault strike is then roughly continuous with the Pleito fault to the southwest and with the Breckenridge fault to the northeast. Although no ground breakage was reported along the Pleito fault in 1952, displacement of the basement rocks may have accompanied or preceded rupture on the White Wolf fault. Aftershocks extended into the Pleito fault zone, but no relevels have been examined west of the 1952 epicenter for any period.

Post-Seismic Deformation

No surface offsets and no near-fault displacement gradients can be seen on the records from any of the six relevel intervals after the 1952 earthquake, as is evident in Figure 10. Although subsidence associated with Edison oilfield obscures the precise nature of the displacement on the footwall block of the White Wolf fault after 1952, the greatest flexure of the uplift, lies at least 10 km northwest of the White Wolf fault. No major discontinuities can be seen across the Garlock fault (Figure 10).

The post-seismic uplift profile can be plausibly but not uniquely modeled by deep slip on shallow-dipping faults extending from the base of those that ruptured in 1952, and this possibility is not excluded by the near-fault post-seismic shear strain changes. This explanation is attractive because post-seismic uplift was greatest where the seismic slip was small. Hence fault slip after the earthquake would tend to equalize the total slip since 1952 at both ends of the fault. Viscoelastic or asthenospheric rebound, on the other hand, should be large where the seismic slip was deepest, in order to tap material that will flow to relieve shear stresses applied during faulting. However, post-seismic uplift in the northeast where the fault was modeled to be 10 km deep, was twice as large as near the epicenter, which is at least two times deeper (Figure 11*a*). Post-earthquake uplift that is exhibited by many large underthrust earthquakes tends to decay roughly exponentially with time and has been interpreted both in terms of deep fault slip and localized viscous relaxation [*Kasahara,* 1975; *Thatcher and Rundle,* 1979; *Wahr and Wyss,* 1980]. This is quite unlike the record for the 1952 earthquake. So while viscoelastic rebound and fault slip cannot be distinguished from the data, deep and widespread fault slip after 1959 appears possible. Since the suitability of a homogeneous elastic half space for modeling slow post-seismic slip is open to question, we did not attempt to fit aseismic surface displacements precisely with dislocations.

The apparent 7–16 km/yr spreading of deformation from the epicentral region to the northeast and the finding that slip took place beneath the epicenter to a depth of about 20–27 km provide evidence for a tentative mechanical link between the earthquake and subsequent regional uplift: deep slip may have followed coseismic upper crustal slip. Creep may have begun in the more ductile material displaced beneath the epicenter during the earthquake or within the first year after the 1952 shock and propagated northeast to the region where seismic slip was confined to more brittle material.

Bakersfield was held fixed for the post-seismic relevels, because it is the most convenient point to which all surveys were tied. The southern terminus of the leveling route from Bakersfield to Gorman can be subjected to comparison by fixing Saugus, 75 km south of the epicenter (Figure 11*b*). The two frequently resurveyed BM's that are closest to each other share the same history of elevation change. In other words, Bakersfield and Saugus remained fixed with respect to each other from 1953 through 1974. Ties from Bakersfield to BM Tidal 8 are only available tin 1953/1955, 1965, and 1972. Relative to msl corrected for the eustatic sea level trend, Bakersfield rose 130 ± 48 mm during this period. *Strange* [1981] applied a correction for differential optical refraction to the observed data, and this yields +25 ± 20 mm for Bakersfield relative to Los Angeles (V32) for 1953 to 1972 (add values from Tables 4 and 5 and Figure 12 in *Strange* [1981] to derive this figure). Fixing the elevation for Bakersfield may therefore underestimate the net regional uplift by 145 ± 52 mm, depending on what correction for refraction, if any, should be applied to the observed elevations. Near-fault observations are in no way affected by these assumptions.

Late Quaternary Tectonic Processes

The rate of vertical displacement on the White Wolf fault accelerated dramatically between about 15 m.y. ago and 1.2–0.6 m.y. ago (Figure 14). The onset of the acceleration may be similar for the northwest and southwest margins of the southern California uplift, as *Yeats* [1977] found that rapid uplift at Ventura (VB in Figure 1) began about 0.6 m.y. ago. This change in the style and rate of tectonic deformation may reflect the opening of the Gulf of California, and creation of the southern California transform faults during the last three to five million years.

During both the late Quaternary and the 48 year geodetic epoch, the rate of vertical fault slip has been about three times greater than the rate of emergence of the hanging-wall block (Figure 14). During approximately the last million years, then, the White Wolf footwall block, which lies between the fault trace and Bakersfield, has been subsiding below sea level at twice the rate of emergence. The southern San Joaquin Valley has subsided at 3–6 mm/yr during the late Quaternary, and at 5–20 mm/yr during the period of geodetic observation. In contrast to this observation, continued displacement on the modeled White Wolf fault must cause uplift of the hanging-wall block to exceed the subsidence of the footwall block, a product of the reverse dip of the fault. Thus some additional, perhaps inelastic process of strain accumulation must help to create the pronounced subidence in the southern San Joaquin Valley. In this respect the deformation is similar to that observed in fore-arc basins along subduction zones, where unusually thick sedimentary prisms form at the convergent boundary.

The southern San Joaquin Valley is deepest where the coseismic reverse slip was greatest, in the region of the 1952 epicenter. The asymmetrical form of the valley syncline can be seen on the structure contour map of Figure 13*a*. In addition, the left-lateral offset of the marker bed in the Miocene Santa Margarita Formation is about 5 km where the vertical separation of the Santa Margarita, from Figure 12, is also 5 km. Thus the ratio of reverse to lateral slip since Miocene time has been about 1:1 at the location where the modeled slip ratio was 1.2:1 during the 1952 earthquake. The relative components of displacement in 1952 may therefore be characteristic of the geologic displacement; the 1952 event may be representative of Quaternary tectonic behavior of the fault.

We have deduced a 170- to 450-year recurrence interval for earthquakes with throw similar to that in 1952 on the White Wolf fault under the tenuous assumptions that the late Quaternary displacement rate persists today, and that the contribution of aseismic fault slip to the throw is small. The rate of emergence of the hanging wall block during the past 48 years is about three to four times greater than that since the late Quaternary, as shown in Figure 14. This difference in rate probably reflects the dominance of the 1952 earthquake during the geodetic epoch. We have also presented evidence for significant aseismic deformation that may be caused by deep fault slip. If aseismic reverse slip does accumulate, then we have underestimated the recurrence interval by about 25%.

The cycle of strain accumulation and release on the San Andreas fault may control or influence that for adjacent or adjoining subsidiary faults. With the preceding qualifications regarding the recurrence interval in mind, consider the following: The nearby San Andreas fault (160- to 250-year apparent recurrence [*Sieh*, 1978*a*]) and the White Wolf fault (170- to 450-year inferred average recurrence) may have similar recurrence intervals despite the 5–6 times greater rupture length and 4–6 times greater slip rate of the San Andreas fault. We offer two further observations to support this contention: As shown in Figure 13*b*, a 2-m decrease in slip along the San Andreas in 1857 occurred within 30 km of its intersection with the Pleito fault [*Sieh*, 1978*b*]. Strain there may be partially relieved or reduced by earthquakes on the White Wolf or Pleito faults. In addition, in 1952 the lateral slip on the White Wolf fault only 30 km from the San Andreas was 2 m; the amount of slip decreased with distance from the major right-lateral fault. The frequency and character of ruptures on the Quaternary White Wolf fault may therefore be coupled to the cycle of strain accumulation and release on the San Andreas fault.

Acknowledgments. This work benefited enormously from the guidance and editorial acumen of Robert O. Castle. We are fortunate to have had the insight, advice, and critical reviews of Bernard Hallet, Malcolm Clark, Amos Nur, Kerry Sieh, and J. C. Savage. Masataka Ando graciously provided his dislocation program for our use. We are indebted to Michael Elliot, Jack Church, and members of the Vertical Networks Branch of the National Geodetic Survey for helping us assemble the relevels. One of us (R.S.) would like to thank Stanford University for the generous support received while a student there.

REFERENCES

Allen, C. R., P. St. Amand, C. F. Richter, and J. M. Nordquist, Relationship between seismicity and geologic structure in the southern California region, *Bull. Seismol. Soc.Am., 55*, 753–797, 1965.

Ben-Menahem, A., Renormalization of the magnitude scale, *Phys. Earth Planet. Interiors, 15*, 315–340, 1977.

Bomford, G., *Geodesy*, pp. 226–280, Oxford University Press, London, 1971.

Branner, J. C., The Tejon Pass earthquake of October 22, 1916, *Bull. Seismol. Soc. Am., 17*, 51–59, 1917.

Buchanan-Banks, J. M., R. O. Castle, and J. I. Ziony, Elevation changes in the central Transverse Ranges near Ventura, California, *Tectonophysics, 29,* 113–125, 1975.

Buwalda, J. P., Geology of the Tehachapi Mountains, California, Geology of southern California, *Calif. Div. Mines Geol. Bull., 170*(2), 131–142, 1954.

Buwalda, J. P., and P. St. Amand, Geological effects of the Arvin-Tehachapi earthquake, *Calif. Div. Mines Geol. Bull., 171,* 41–56, 1955.

Callaway, D. C., Correlation section 17, San Joaquin Valley: Kingsburg to Tejon Hills, Pacific section, *Am. Assoc. Petrol. Geol.,* 1969.

Castle, R. O., Leveling surveys and the southern California uplift, *Earthquake Inform. Bull., 10,* 88–92, 1978.

Castle, R. O., J. P. Church, and M. R. Eliot, Aseismic uplift in Southern California, *Science, 192,* 251–253, 1976.

Davis, P., J. Smith, G. J. Kukla, and N. D. Opdyke, Paleomagnetic study at a nuclear power plant site near Bakersfield, California, *Quaternary Res., 7,* 380–397, 1977.

Dunbar, W. S., The determination of fault models from geodetic data, Ph.D. dissertation, Stanford Univ., Stanford, Calif., 1977.

Dunbar, W. S., D. M. Boore, and W. Thatcher, Pre-, co-, and postseismic strain changes associated with the 1952 $M_L = 7.2$ Kern County, California, earthquake, *Bull. Seismol. Soc. Am., 70,* 1893–1905, 1980.

Federal Geodetic Control Committee, *Classification, Standards of Accuracy, and General Specifications of Geodetic Control Surveys,* Nat. Oceanic and Atmos. Admin., Rockville, Md., 1974.

Federal Geodetic Control Committee, *Specifications to Support Classification, Standards of Accuracy, and General Specifications of Geodetic Control Surveys,* Nat. Oceanic and Atmos. Admin., Rockville, Md., 1975.

Frank, F. C., Deduction of earth strains from survey data, *Bull. Seismol. Soc. Am., 546,* 35–42, 1966.

Freund, L. B., and D. M. Barnett, A two-dimensional analysis of surface deformation due to dip-slip faulting, *Bull. Seismol. Soc. Am., 66,* 670–675, 1976.

Gutenberg, B., The first motion on longitudinal and transverse waves of the main shock and the direction of slip, *Calif. Div. Mines Geol. Bull., 171,* 165–170, 1955.

Heiskanen, W. A., and H. Moritz, *Physical Geodesy,* W. H. Freeman, San Francisco, Calif., 1967.

Hicks, S. C., and J. F. Crosby, An average, long period, sea-level series for the United States, *Tech. Memo. 15,* Nat. Oceanic and Atmos. Admin., Rockville, Md., 1975.

Hileman, J. A., C. R. Allen, and J. M. Nordquist, Seismicity of the southern California Region, 1 January 1932 to 31 December 1972, *Contrib. 2385,* Seismol. Lab., Calif. Inst. of Technol., Pasadena, 1973.

Hillhouse, J., and A. Cox, Brunhes-Matuyama polarity transition, *Earth Planet. Sci. Lett., 29,* 51–64, 1976.

Hoots, H. W., Geology and oil resources along the Southern San Joaquin Valley, California, *U.S. Geol. Surv. Bull., 812-D,* 243–338, 1930.

Ishida, M., and H. Kanamori, Temporal variation in seismicity and spectrum of small earthquakes preceding the 1952 Kern County, California, earthquake, *Bull. Seismol. Soc. Am., 70,* 509–527, 1980.

Izett, G. A., C. W. Naeser, and J. D. Obradovich, Fission track age of zircons from an ash bed in the Pico formation (Pliocene and Pleistocene) near Ventura, California, *Geol. Soc. Am. Abstr. Programs, 6,* 197, 1974.

Janda, R. J., Quaternary alluvium near Friant, California, *Int. Union Quat. Res. 7th Congr. Guideb., 128,* 1965.

Jungels, P. H., and G. A. Frazier, Finite element analysis of the residual displacements for an earthquake: Source parameters for the San Fernando earthquake, *J. Geophys. Res., 78,* 5062–5083, 1973.

Kasahara, K., Aseismic faulting following the 1973 Nemuro-oki earthquake, Hokkaido, Japan (a possibility), *Pure Appl. Geophys., 113,* 127–139, 1975.

Lajoie, K. R., J. P. Kern, J. F. Wehmiller, G. L. Kennedy, S. A. Mathieson, A. M. Sarna-Wojcicki, R. F. Yerkes, and P. F. McCroy, Quaternary marine shorelines and crustal deformation, San Diego to Santa Barbara, California, in *Geological Excursions in the Southern California Area,* edited by P. L. Abbot, pp. 1–16, San Diego State University, San Diego, Calif., 1979.

Lofgren, B. E., Land subsidence due to ground-water withdrawal, Arvin-Maricopa area, California, *U.S. Geol. Surv. Prof. Pap., 437-0,* 1975.

Mansinha, L., and D. E. Smylie, The displacement fields on inclined faults, *Bull. Seismol. Soc. Am., 61,* 1433–1440, 1971.

Mark, R. K., J. C. Tinsley, E. B. Newman, T. D. Gilmore, and R. O. Castle, An assessment of the accuracy of the geodetic measurements that define the southern California uplift, *J. Geophys. Res., 86,* 2783–2808, 1981.

Sarna-Wojcicki, A., Correlation of late Cenozoic tuffs in the central Coast Ranges of California by means of trace and minor-element chemistry, *U.S. Geol. Surv. Prof. Pap., 972,* 1976.

Savage, J. C., and R. O. Burford, Strain accumulation in California, *Bull. Seismol. Soc. Am., 60,* 1877–1896, 1970.

Seih, K. E., Prehistoric large earthquakes produced by slip on the San Andreas fault at Pallett Creek, California, *J. Geophys. Res., 83,* 3907–3939, 1978*a*.

Seih, K. E., Slip along the San Andreas fault associated with the great 1857 earthquake, *Bull. Seismol. Soc. Am., 68,* 1421–1428, 1978*b*.

Stein, R. S., Discrimination of tectonic displacement from slope-dependent errors in geodetic leveling from Southern California 1953–1979, in *Earthquake Prediction, An International Review, Maurice Ewing Ser.,* vol. 4, edited by D. W. Simpson and P. G. Richards, AGU, Washington, D. C., 1981.

Stein, R. S., and S. Silverman, Random elevation-correlated changes in southern California leveling (abstract), *Eos Trans. AGU, 61,* 366, 1980.

Strange, W. E., The impact of refraction correction on leveling interpretations in southern California, *J. Geophys. Res., 86,* 2809–2824, 1981.

Thatcher, W., Strain accumulation and release mechanism of the 1906 San Francisco earthquake, *J. Geophys. Res., 80,* 4862–4872, 1975.

Thatcher, W., Episodic strain accumulation in southern California, *Science, 194,* 691–695, 1976.

Thatcher, W., Horizontal crustal deformation from historic geodetic measurements in southern California, *J. Geophys. Res., 84,* 2351–2370, 1979.

Thatcher, W., and J. B. Rundle, A model for the earthquake cycle in underthrust zones, *J. Geophys. Res., 84,* 5540–5556, 1979.

Toppozada, T. R., D. L. Parke, and C. T. Higgins, Seismicity of California 1900–1931, *Calif. Div. Mines Geol. Spec. Rep., 135,* 1978.

Vaníček, P., E. I. Balazs, and R. O. Castle, Geodetic leveling and its applications, *Rev. Geophys. Space Phys., 18,* 505–524, 1980.

Wahr, J., and M. Wyss, Interpretation of postseismic deformation with a viscoelastic relaxation model, *J. Geophys. Res., 85,* 6471–6477, 1980.

Webb, G. W., Stevens and earlier Miocene turbidite sands, San Joaquin Valley California, in *Late Miocene Geology and New Oil Fields of the Southern San Joaquin Valley, AAPG-SEG-SEPM Pacific Section Guidebook,* American Association of Petroleum Geologists, Tulsa, Okla., 1977.

Wehmiller, J. E., K. R. Lajoie, K. A. Kvenvolden, E. Peterson, D. F. Belknap, G. L. Kennedy, W. D. Addicott, J. G. Vedder, and R. W. Wright, Correlation and choronology of Pacific coast marine terrace deposits of continental United States by fossil amino acid stereochemistry, *U.S. Geol. Surv. Open File Rep., 77-680,* 1977.

Wood, S. H., and M. R. Elliot, Early 20th-century uplift of the northern Peninsular Ranges province of southern California, *Tectonophysics, 52,* 249–265, 1979.

Yeats, R. S., High rates of vertical crustal movement near Ventura, California, *Science, 196,* 295–298, 1977.

(Received June 22, 1979;
revised December 8, 1980;
accepted December 16, 1980.)